Astronomy & Astrophysics

L~ETTER~ TO THE E~DITOR~

Evidence for globular cluster collapse after a dwarf-dwarf merger: A potential nuclear star cluster in formation

J. Román[1,2,3], P. M. Sánchez-Alarcón[2,3], J. H. Knapen[2,3], and R. Peletier[1]

[1] Kapteyn Astronomical Institute, University of Groningen, PO Box 800, 9700 AV Groningen, The Netherlands
   e-mail: jromanastro@gmail.com
[2] Instituto de Astrofísica de Canarias, c/ Vía Láctea s/n, 38205 La Laguna, Tenerife, Spain
[3] Departamento de Astrofísica, Universidad de La Laguna, 38206, La Laguna, Tenerife, Spain

ABSTRACT

Direct observational evidence for the creation of nuclear star clusters (NSCs) is needed to support the proposed scenarios for their formation. We analysed the dwarf galaxy UGC 7346, located in the peripheral regions of the Virgo Cluster, to highlight a series of properties that indicate the formation of a NSC caught in its earlier stages. First, we report on remnants of a past interaction in the form of diffuse streams or shells, suggesting a recent merging of two dwarf galaxies with a 1:5 stellar mass ratio. Second, we identify a number of globular cluster (GC) candidates that are broadly compatible in colour with the main component that is both more extended and more massive. Strikingly, we find these GCs candidates to be highly concentrated towards the centre of the galaxy ($R_{GC} = 0.41 R_e$). We suggest that the central concentration of the GCs is likely produced by the dynamical friction of this merger. This would make UGC 7346 a unique case of a galaxy caught in the earlier stages of NSC formation. The formation of NSCs due to collapse of GCs by dynamical friction in dwarf mergers would provide a natural explanation of the environmental correlations found for the nucleation fraction for early-type dwarf galaxies, whereby denser environments host galaxies with a higher nucleation fraction.

Key words. galaxies: dwarf – galaxies: star clusters: general – galaxies: structure

1. Introduction

Nuclear star clusters (NSCs) are extremely compact stellar structures located in the central regions of so-called nucleated galaxies (for a recent review, see Neumayer et al. 2020). The presence of NSCs in galaxies was first noticed in early studies in the Virgo cluster (Reaves 1983; Caldwell 1983; Binggeli et al. 1987). A large number of galaxies in different environments have since been observed to understand the properties of NSCs. The fraction of nucleated galaxies is strongly dependent on their mass and morphology, reaching a maximum nucleation fraction of about 80% for $M_\star = 10^9 M_\odot$, decreasing for higher and lower masses (Neumayer et al. 2020, and references therein). The fraction of nucleated galaxies also depends on the environment, with the fraction higher in denser environments (Sánchez-Janssen et al. 2019; Su et al. 2022; Carlsten et al. 2022). The intrinsic properties of NSCs correlate strongly with those of their host galaxy (Balcells et al. 2003, 2007; Côté et al. 2006; Ferrarese et al. 2006).

Despite exhaustive studies trying to unravel how NSCs are formed, a complete picture of their formation mechanism has not yet emerged (Neumayer et al. 2020), however, two different scenarios have been deemed as plausible. The coalescence of globular clusters (GCs) by dynamical friction is the most widely established mechanism for the formation of NSCs (e.g., Tremaine et al. 1975; Capuzzo-Dolcetta 1993; Lotz et al. 2001; Oh & Lin 2000). However, the presence of young stellar populations in NSCs, especially in late-type galaxies (e.g., Bender et al.

2005; Lu et al. 2013; Georgiev & Böker 2014; Carson et al. 2015) but also in early-type galaxies (Nguyen et al. 2017, 2019), suggests a potential contribution on the part of in situ star formation in NSCs. There is a lot of evidence that indicates a transition in the properties of NSCs in galaxies for a mass threshold of $M_\star = 10^9 M_\odot$ (see Neumayer et al. 2020, and references therein). Galaxies below this mass would have a NSC formation mechanism dominated by GC coalescence, while for masses above this threshold, in situ formation would be dominant. This statement is supported by a recent analysis of the star formation histories of NSCs by Fahrion et al. (2021).

Despite the clear evidence suggesting these formation channels for NSCs, there is still no direct observational evidence showing a case where a NSC is caught being formed (however, see Schiavi et al. 2021, for the case of a nuclear merger in its later stages). The very short timescales on which NSCs are expected to be formed (e.g., Capuzzo-Dolcetta & Miocchi 2008a,b) lower the chances of observing a merger of GCs into a NSC. Additionally, some properties of NSCs remain to be explained under these two formation mechanisms. For instance, the correlation between the fraction of nucleated galaxies and the environment (e.g., Sánchez-Janssen et al. 2019; Su et al. 2022; Carlsten et al. 2022) offers no easy explanation under these proposed mechanisms, as they are internal to the hosts.

In this Letter, we base our analysis on the dwarf elliptical (*dE*) galaxy UGC 7346. We argue that it is a case of a dwarf-dwarf merger inducing the collapse of its GCs and, thus, we consider it to be in the early stages of NSC formation. We assume a distance for UGC 7346 of 16.5 Mpc (Mei et al. 2007),

implying a distance modulus of $m - M = 31.09$ mag and a scale of 0.080 kpc arcsec^{-1}. All photometric quantities are extinction-corrected following Schlafly & Finkbeiner (2011). We use the AB photometric system throughout this work.

2. Data

We use publicly available data from the Dark Energy Camera Legacy Survey (DECaLS; Dey et al. 2019). This survey provides deep g, r, and z band images. We downloaded stamps centred on UGC 7346 in all bands via webpage of the survey[1]. We use the seventh data release. The limiting surface brightness calculated following the method by Román et al. (2020) are 28.9, 28.2, and 27.3 mag arcsec^{-2} [3σ; 10×10 arcsec] for the g, r, and z bands, respectively.

We explored the existence of other datasets, but found no data available in the CFHT Science Archive or the Hubble Legacy Archive. We found data from Pan-STARRS, however because they are shallower and less optimally processed compared to DECaLS data, we discard their use.

3. Analysis

3.1. Photometric decomposition

The surface brightness profile of UGC 7346 is characterised by a central concentration of bluer light and a redder flat profile in the outer regions (Fig. 1). We modelled the structure of UGC 7346 with a structural analysis with Sersic (Sersic 1968) models using the IMFIT software (Erwin 2015). Two different settings were employed: single Sersic and double Sersic models. For the fitting, we first calculated the ellipticity, position angle, and central coordinates of the models on the $g+r+z$ image. These parameters are subsequently fixed for the fitting of the individual bands, leaving the rest of the parameters free. The fitting was carried out with a chi-square minimization using the IMFIT default parameters.

In Fig. 1, we plot the g band surface brightness profile of UGC 7346, together with the fitted single and double Sersic models, as well as the $g - r$ colour profile (we omitted the $r - z$ colour due to the low signal to noise of the z-band). The single Sersic model produces slight deviations from the profile of UGC 7346, while the double Sersic model fits it better. In order to appreciate more clearly the differences in the surface brightness profiles between the fitted models and UGC 7346, we subtracted the models from the profile of UGC 7346 (Fig. 1, right panel). The single Sersic model has larger deviations from the UGC 7346 profile with a v-shape feature with vertex at approximately 20 arcsec. On the other hand, the difference with the double Sersic model remains approximately constant around 0, with slight undulations, which as we will discuss later are due to the substructure in UGC 7346 has underneath. The models deviate significantly at high radius (>80 arcsec), probably due to sky oversubtraction in the Legacy Survey data.

Regarding the $g - r$ colour profile, both the single and double Sersic models reproduce the central colour of UGC 7346. However, in the outer parts, the single model fails to reproduce the redder colour of UGC 7346 beyond 50 arcsec. Based strictly on the analysis of the surface brightness profiles, the double Sersic model fits more accurately the structure of UGC 7346. As we discuss in the following, there are supplementary arguments to support a double Sersic component in UGC 7346.

In the lower panels of Fig. 1, we show the two individual components of the double Sersic model. We refer to the components as 'main' and 'secondary', according to the established structural parameters, in which the main model dominates in luminosity and extension over the secondary model. Both models have coincident centrers. In Table 1 we show their structural properties. The colours of the main model are $g - r = 0.60 \pm 0.06$ mag and $r - z = 0.27 \pm 0.12$ mag, and for the secondary model, we have $g - r = 0.50 \pm 0.11$ mag and $r - z = 0.64 \pm 0.22$ mag. With this modelling, the structure of UGC 7346 is explained by a bluer component of smaller extent and luminosity that dominates the flux in the central region, while the dominant component is redder and of larger extent. The individual profiles of these main and secondary components of the double Sersic model (Fig. 1) show how there is a transition in the colour profile from the approximate colour of the secondary model in the central region to the colour of the main component at higher radius. These circumstances confirm that the modeling with these two components is coherent and that the structure of UGC 7346 can be explained with two different stellar components with different and distinctive colours.

While the models used for each component are synthetic Sersic models, there is an underlying substructure. This emerges in the images after subtracting the models from UGC 7346 and is also noticeable in the residual profile between UGC 7346 and the models (upper-right panel of Fig. 1). We find certain fluctuations up to a radius of 20 arcsec, which we associate with the streams or shells found in the central region of UGC 7346. We can also identify a bump in flux produced by a quasi-circular structure located at approximately 60 arcsec. We rule out that the residual structures located in the central region are a product of incorrect modeling, since they appear regardless of the fitted model and are even visible in the original image without model subtraction. On the other hand, we cannot rule out that the almost circular structure located at approximately 60 arcsec is some kind of artifact since it is located in the external regions, close to where the sky is oversubtracted in the data. Better and deeper imaging with no oversubtraction of the sky background will be needed to confirm or discard this outer stream.

The signs of interaction in the form of streams or shells, together with the existence of two stellar components with distinctive colours, indicate that UGC 7346 is most likely the result of a dwarf-dwarf merger. This statement is supported by previous work. Benítez-Llambay et al. (2016) showed from cosmological simulations that the product of dwarf-dwarf mergers is the presence of a bluer and more concentrated stellar component surrounded by a redder and older one in dwarf spheroidals. Additionally, Chung et al. (2019) showed that two blue-cored dwarfs in Virgo (as is the case of UGC 7346) are the product of dwarf-dwarf mergers by means of a kinematic analysis of their stellar component with spectroscopy. Therefore, the observational evidence we have clearly points to a 1:5 (see Table 1) dwarf-dwarf merger as responsible for the peculiar structure of UGC 7346.

3.2. Globular cluster candidates

A significant concentration of point sources in the central region of UGC 7346 suggests the presence of a GC system. In order to make a catalogue of GC candidates, we carried out aperture photometry with the available g, r, and z bands. This combination of bands is efficient for the detection of GC candidates (see Román et al. 2021, who used similar data). In Appendix A, we describe in the process for selecting point sources compatible

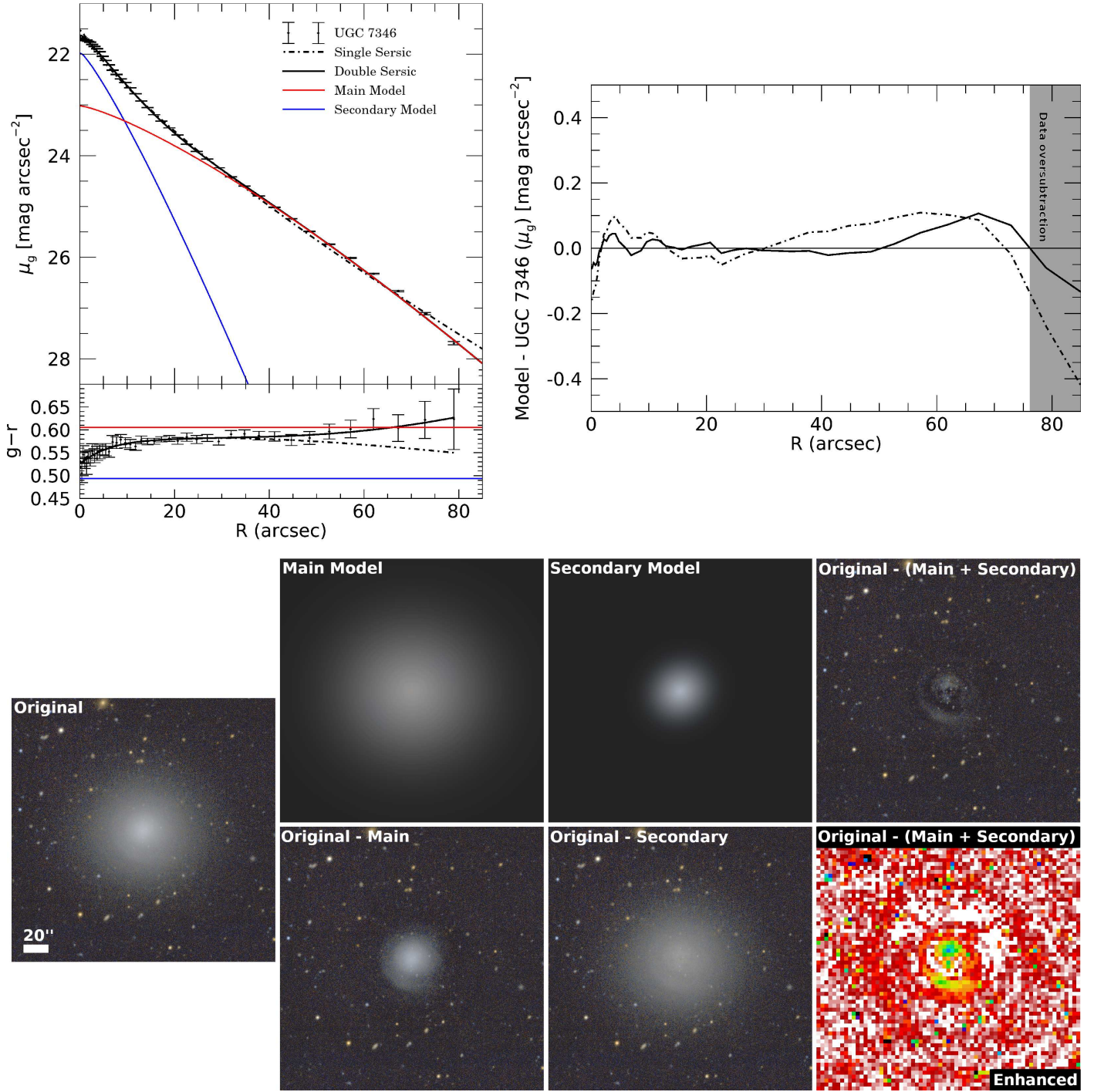---

[1] https://www.legacysurvey.org

Fig. 1. Photometric analysis and decomposition of UGC 7346. Upper left panel: surface brightness profile in g band and $g - r$ colour profile for UGC 7346 and models (see text). Upper right panel: residual after subtracting the surface brightness profile of UGC 7346 from the models. Bottom: modelling of UGC 7346 in two different Sersic components. The left image is the original image. The upper centre images are the two fitted Sersic models, showing the corresponding residuals of these models in the lower central images. The result of subtracting the sum of the two models is shown in the right images. The enhanced residual image is produced by binning the $g + r$ residual image to a size of 10x10 original pixels and using a high contrast false colour, allowing a greater appreciation of the lower surface brightness structures. The rest of the colour images are constructed using g and r bands. All images have a size of 3.6×3.6 arcmin. North is up, east to the left.

with GC candidates, together with an analysis of the expected luminosity function of GCs for UGC 7346. An important point in this discussion is the fact that that we selected a range in the $g - r$ vs. $r - z$ colour space for the detection of GC candidates that is compatible with the colours of the two stellar components discussed in the previous section, namely, the potential GCs of these two stellar components.

In Fig. 2, we show the results of this selection of GC candidates. In the left panel, we show the colour of the detected GC candidates around UGC 7346. The GC candidates are distributed in the region compatible with the colour of the main model. We indicate the average colour of all the 14 GC candidates located within three times the effective radius of the main model with a black symbol. We use a weighted mean taking into account

Table 1. Structural parameters of the two-component Sersic modeling for UGC 7346.

Parameter	Main model	Secondary model
R_e [arcsec]	31.9 ± 1.7	11.0 ± 1.2
Sérsic index	0.78 ± 0.06	0.84 ± 0.05
Axis ratio	0.94 ± 0.01	0.91 ± 0.01
Position angle [deg]	89 ± 3	125 ± 7
g-band [mag]	14.33 ± 0.04	15.75 ± 0.08
r-band [mag]	13.73 ± 0.04	15.25 ± 0.08
z-band [mag]	13.46 ± 0.11	14.61 ± 0.20
L_g [mag]	-16.76 ± 0.04	-15.34 ± 0.08
$M_\star$ [$M_\odot$]	$1.2 \pm 0.2 \times 10^9$	$2.4 \pm 0.8 \times 10^8$

Notes. Stellar masses are calculated using predictions by Roediger & Courteau (2015) with the g and r bands.

photometric errors. The average colour of the GC candidates is only compatible with the main model, which confirms that the GCs belong to this stellar component. In the right panel, we show the distribution of the GC candidates in UGC 7346. We overplot the effective radius of both stellar components or models discussed above. The high concentration of GC candidates in the central region of UGC 7346 is discussed later in this work.

In Fig. 3, we show an image similar to the right panel of Fig. 2, but this time overplotting the GC candidates on the residual $g+r$ image in high contrast after having subtracted the models and zooming in on the central region. We find that the position of the GCs coincides remarkably well with regions of flux overdensity in this residual image. Of the nine GC candidates located within the main model effective radius, eight of them are located where a residual positive flux is found after model subtraction.

4. Discussion

The analysis carried out in the previous section shows properties in UGC 7346 that are atypical in terms of two aspects. By decomposing the galaxy light of UGC 7346 we find that its morphology is explained by the superposition of two different stellar components with distinctly different colours (see Fig. 1). Additionally, by analyzing the residual images after the subtraction of the models we find what look like remnants of an interaction in the form of streams or shells. In this regard, we comment on the presence of substructures with spiral patterns in early-type dwarfs in the recent work by Michea et al. (2021, 2022). These structures are found underneath the main smooth component of dwarf galaxies in the Virgo and Fornax clusters; Smith et al. (2021) have proposed that they are due to tidal forces causing an underlying disk component to emerge.

We argue that the substructure found in UGC 7346 is qualitatively different from those structures. First, UGC 7346 has two clearly distinct stellar components and not only one dominant smooth component. In addition, the residual substructure in UGC 7346 is considerably more asymmetric than the early-type dwarf structures by Michea et al. (2021, 2022), which are fairly symmetric. We considered the possibility that the residuals could be a potential dust lane. The available optical SDSS spectra for UGC 7346[2] show a passive population with no signs of star formation. We did not find HI detection in UGC 7346 nor mid-IR counterparts to the features in the unWISE data

(Lang 2014). These arguments together, including additional arguments discussed in Sect. 3.1, suggest that the overall structure of UGC 7346 is due to a dwarf-dwarf merger. This is in itself of high interest since few examples of early-type dwarf on-going mergers are found in the literature, with most dwarf-dwarf mergers showing high star formation activity (Stierwalt et al. 2017; Paudel et al. 2018; Kado-Fong et al. 2020; Zhang et al. 2020; Egorova et al. 2021).

Another remarkable aspect is the existence of a highly concentrated system of GCs with that colours that are broadly compatible with the main model component. Given the GC candidates found within three times the effective radius of the main model, we estimate a half-number radius (R_{GC}) for the GC system of approximately 13 arcsec. This implies $R_{GC} = 0.41 R_e$, which is certainly a strong anomaly, since both the radial and azimuthal GC distributions follow those of the stars in dwarf galaxies, with typical values for R_{GC}/R_e of the order of unity or above (see Saifollahi et al. 2022, and references therein). We note that even assuming a single Sersic model to define the structure and effective radius of UGC 7346, the concentration of the GC candidates would be $R_{GC} = 0.50 R_e$, so the very high concentration of the GC candidates is model-independent.

We would like to point out that some of the specific properties of UGC 7346 have been previously observed in other galaxies. For instance, the presence of blue cored dE in clusters is frequent and well known (Urich et al. 2017; Hamraz et al. 2019). However, a complete analysis addressing both the presence of stellar subcomponents, the presence of substructure, and the distribution of globular clusters, does not exist in the literature. Considering the excellent data available in the nearby Virgo, Fornax and Coma clusters, this potential study could offer compatible cases to those we present in UGC 7346.

We suggest that the two coincident anomalies in UGC 7346, a dwarf-dwarf merger and the high concentration of its GCs, may be related to each other. A straightforward interpretation of the points discussed above would suggest that the dynamical friction produced by the ongoing dwarf-dwarf merger is collapsing the GCs towards the centre of UGC 7346. Indeed, simulations suggest that tidal forces in dwarf galaxies are sufficient to trigger a collapse of the GC system, and Oh & Lin (2000) were able to produce such a central concentration of GCs for some initial conditions. This could be the case for UGC 7346. In principle, a merger event would provide a tidal field intense enough to create this collapse of the GCs by dynamical friction. However, in the literature we did not find a specific case of cosmological simulations of dwarf-dwarf mergers and their impact on the globular cluster system.

To explore the hypothetical result of the merger of the GCs observed in the central region of UGC 7346, we calculated the total luminosity of this set of GCs, selecting those nine GC candidates that are inside the effective radius of the main model (see Fig. 3). The total integrated luminosity of this set of nine GC candidates is $L_g = -10.2$ mag. Considering the total mass of UGC 7346, $M_\star = 1.4 \times 10^9 M_\odot$, the luminosity of the hypothetical NSC formed by merging these GCs is in excellent agreement with the observed correlations between host galaxy mass and NSC luminosity (see Neumayer et al. 2020). There are, however, some caveats in this calculation. First, we do not know with certainty whether all or only some of the GC candidates in the selected region would eventually merge. Additionally, our photometric data are not complete to the entire GC luminosity function of UGC 7346. In Appendix A, we show that the depth of our data allows us to map approximately half of the expected GCs in UGC 7346. Nevertheless, it is expected that these

---

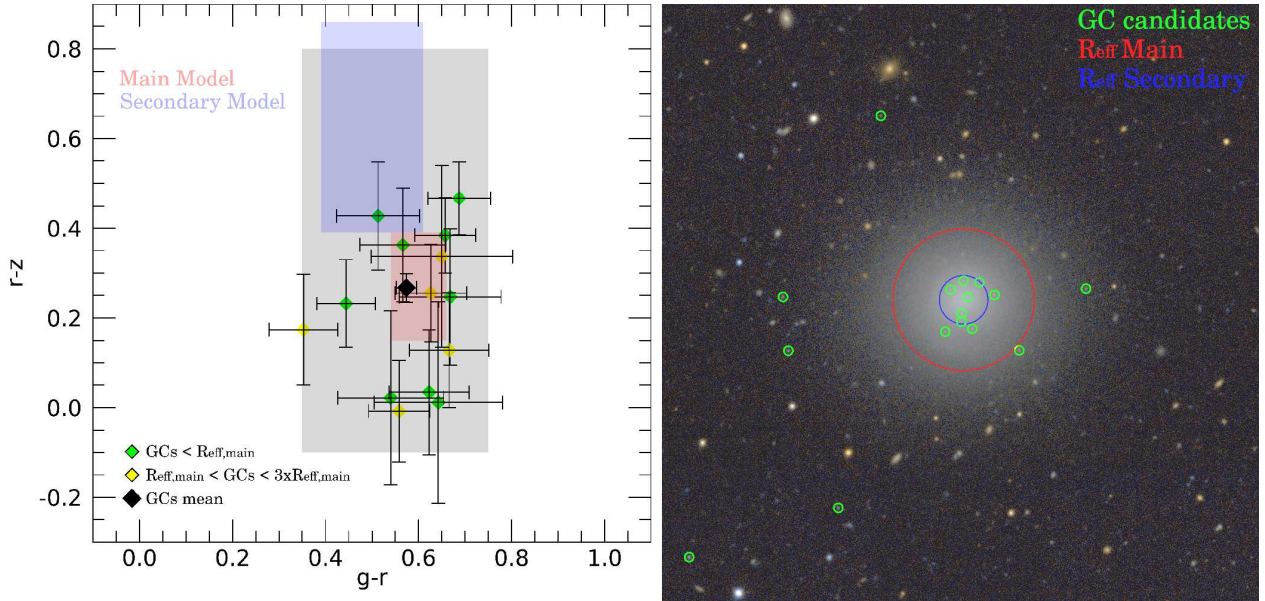[2] http://skyserver.sdss.org/dr16/en/tools/explore/Summary.aspx?id=1237668624622944312

Fig. 2. Analysis of GC candidates around UGC 7346. Left panel: $g - r$ vs. $r - z$ map showing the colour of detected GC candidates and the colours of the main and secondary Models (red and blue rectangles, respectively). The gray rectangle marks the colour space explored for GC candidate detection. GCs are differentiated by green colour (within one effective radius of the main model) and yellow colour (between one and three effective radii of the main model). Right panel: composite colour image (4.5 × 4.5 arcmin) with g and r bands of UGC 7346. GC candidates detected by the selection criteria are plotted with green circles. The effective radii of the main and secondary models are indicated by the red and blue circles, respectively.
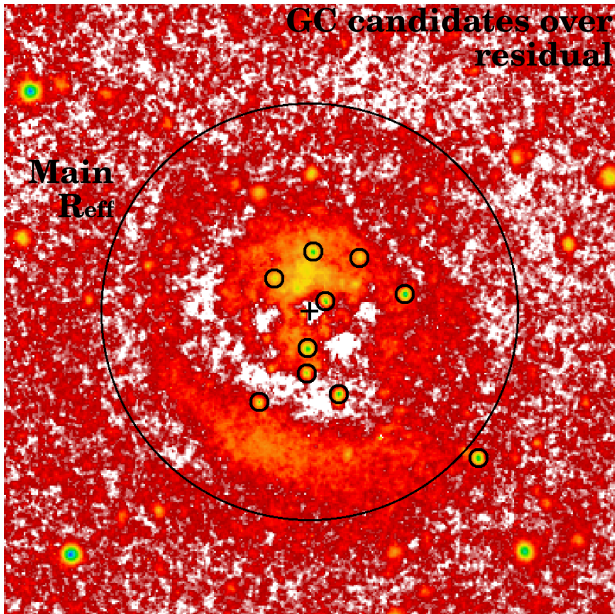

Fig. 3. High-contrast view of the location of the GC candidates (small black circles) on the residual $g + r$ image after subtracting the models discussed in Sect. 3.1. We mark the centre of UGC 7346 with a black cross. The stamp is 70 arcsec sideways over the central region of UGC 7346. The image has been smoothed with the Fully Adaptive Bayesian Algorithm for Data Analysis (FABADA; Sanchez-Alarcon & Ascasibar Sequeiros 2022) software, enhancing the diffuse emission while preserving the original resolution.

undetected GCs of low luminosity – which could potentially merge as well – would contribute little to the luminosity of the hypothetical NSC being formed. Therefore, we can conclude that the hypothetical NSC formed by the merging of the GC can-

didates found in the central region of UGC 7346 would have properties that are compatible with the NSCs and their hosts observed in the literature.

It is also interesting to explore the impact of dwarf-dwarf mergers as a viable channel for the formation of NSCs. Cosmological simulations show that dwarf-dwarf mergers are undoubtedly a common phenomenon (Deason et al. 2014) and dwarfs typically undergo one major and one minor merger in their evolution (Martin et al. 2021). Assuming that dwarf merging is a viable channel to induce the collapse of GCs and the subsequent formation of an NSC, this would provide a natural explanation for the correlations between nucleation fraction and environmental density (e.g., Sánchez-Janssen et al. 2019; Su et al. 2022; Carlsten et al. 2022). In a straight forward argumentation, we can assume that a higher environmental density would produce a higher probability of interactions or merging between dwarf galaxies, thus explaining this correlation. The merging of two dwarfs could even explain the presence of young populations found in NSCs, since both stellar components of the minor component could potentially be younger, or the possible presence of gas could promote in situ star formation. While this scenario is somewhat speculative, we consider it of great interest to explore it in detail. Thus, future theoretical and observational works could confirm whether dwarf mergers do indeed serve as a viable channel for the formation of NSCs.

To conclude, we consider UGC 7346 to be an object of great interest for follow-up observations. First of all, our analysis of its GC system shows that we are limited by point source detections, so that deeper and higher resolution observations would show a larger number of GCs. Additionally, spectroscopic studies of both the GCs and the stellar components would offer the ability to provide dynamical information of the system and a better analysis of its stellar populations – as keys to confirming the hypothesis that the fate of the GCs in UGC 7346 is to merge and ultimately produce a NSC.

References

Arca-Sedda, M., & Capuzzo-Dolcetta, R. 2014, MNRAS, 444, 3738
Balcells, M., Graham, A. W., Domínguez-Palmero, L., et al. 2003, ApJ, 582, L79
Balcells, M., Graham, A. W., & Peletier, R. F. 2007, ApJ, 665, 1084
Bender, R., Kormendy, J., Bower, G., et al. 2005, ApJ, 631, 280
Benítez-Llambay, A., Navarro, J. F., Abadi, M. G., et al. 2016, MNRAS, 456, 1185
Bertin, E., & Arnouts, S. 1996, A&AS, 117, 393
Binggeli, B., Tammann, G. A., & Sandage, A. 1987, AJ, 94, 251
Caldwell, N. 1983, AJ, 88, 804
Capuzzo-Dolcetta, R. 1993, ApJ, 415, 616
Capuzzo-Dolcetta, R., & Miocchi, P. 2008a, ApJ, 681, 1136
Capuzzo-Dolcetta, R., & Miocchi, P. 2008b, MNRAS, 388, L69
Carlsten, S. G., Greene, J. E., Beaton, R. L., et al. 2022, ApJ, 927, 44
Carson, D. J., Barth, A. J., Seth, A. C., et al. 2015, AJ, 149, 170
Chung, J., Rey, S.-C., Sung, E.-C., et al. 2019, ApJ, 879, 97
Côté, P., Piatek, S., Ferrarese, L., et al. 2006, ApJS, 165, 57
Deason, A., Wetzel, A., & Garrison-Kimmel, S. 2014, ApJ, 794, 115
Dey, A., Schlegel, D. J., Lang, D., et al. 2019, AJ, 157, 168
Egorova, E. S., Egorov, O. V., Moiseev, A. V., et al. 2021, MNRAS, 504, 6179
Erwin, P. 2015, ApJ, 799, 226
Fahrion, K., Lyubenova, M., van de Ven, G., et al. 2021, A&A, 650, A137
Ferrarese, L., Côté, P., Dalla Bontà, E., et al. 2006, ApJ, 644, L21
Georgiev, I. Y., & Böker, T. 2014, MNRAS, 441, 3570
Hamraz, E., Peletier, R. F., Khosroshahi, H. G., et al. 2019, A&A, 625, A94
Jordán, A., McLaughlin, D. E., Côté, P., et al. 2007, ApJS, 171, 101
Kado-Fong, E., Greene, J. E., Greco, J. P., et al. 2020, AJ, 159, 103
Lang, D. 2014, AJ, 147, 108
Lotz, J. M., Telford, R., Ferguson, H. C., et al. 2001, ApJ, 552, 572
Lu, J. R., Do, T., Ghez, A. M., et al. 2013, ApJ, 764, 155
Martin, G., Jackson, R. A., Kaviraj, S., et al. 2021, MNRAS, 500, 4937
Mei, S., Blakeslee, J. P., Côté, P., et al. 2007, ApJ, 655, 144
Michea, J., Pasquali, A., Smith, R., et al. 2021, AJ, 161, 268
Michea, J., Pasquali, A., Smith, R., et al. 2022, AJ, 164, 18
Neumayer, N., Seth, A., & Böker, T. 2020, A&A Rev., 28, 4
Nguyen, D. D., Seth, A. C., den Brok, M., et al. 2017, ApJ, 836, 237
Nguyen, D. D., Seth, A. C., Neumayer, N., et al. 2019, ApJ, 872, 104
Oh, K. S., & Lin, D. N. C. 2000, ApJ, 543, 620
Paudel, S., Smith, R., Yoon, S. J., et al. 2018, ApJS, 237, 36
Reaves, G. 1983, ApJS, 53, 375
Rejkuba, M. 2012, Ap&SS, 341, 195
Roediger, J. C., & Courteau, S. 2015, MNRAS, 452, 3209
Román, J., Beasley, M. A., Ruiz-Lara, T., et al. 2019, MNRAS, 486, 823
Román, J., Trujillo, I., & Montes, M. 2020, A&A, 644, A42
Román, J., Castilla, A., & Pascual-Granado, J. 2021, A&A, 656, A44
Saifollahi, T., Zaritsky, D., Trujillo, I., et al. 2022, MNRAS, 511, 4633
Sanchez-Alarcon, P. M., & Ascasibar Sequeiros, Y. 2022, ArXiv e-prints [arXiv:2201.05145]
Sánchez-Janssen, R., Côté, P., Ferrarese, L., et al. 2019, ApJ, 878, 18
Schiavi, R., Capuzzo-Dolcetta, R., Georgiev, I. Y., et al. 2021, MNRAS, 503, 594
Schlafly, E. F., & Finkbeiner, D. P. 2011, ApJ, 737, 103
Sersic, J. L. 1968, Atlas de Galaxias Australes (Argentina: Observatorio Astronomico)
Smith, R., Michea, J., Pasquali, A., et al. 2021, ApJ, 912, 149
Stierwalt, S., Liss, S. E., Johnson, K. E., et al. 2017, Nat. Astron., 1, 0025
Su, A. H., Salo, H., Janz, J., et al. 2022, A&A, 664, A167
Tremaine, S. D., Ostriker, J. P., & Spitzer, L. 1975, ApJ, 196, 407
Urich, L., Lisker, T., Janz, J., et al. 2017, A&A, 606, A135
Villegas, D., Jordán, A., Peng, E. W., et al. 2010, ApJ, 717, 603
Zhang, H.-X., Smith, R., Oh, S.-H., et al. 2020, ApJ, 900, 152

Appendix A: Properties of GC candidates

In this section, we describe the process for selecting GC candidates and their properties. To screen GC candidates we use the model-subtracted images (discussed in Section 3.1) for cleaner point source photometry. We use SExtractor (Bertin & Arnouts 1996) to perform photometry with an aperture of 2.1 arcsec, ~2 times the FWHM of the data, which is 1.1 arcsec in the r band. We used SExtractor in dual mode, with a detection threshold of 5σ, using the $g+r$ image as the detection image to measure photometry in the individual g, r and z bands. We filtered out point sources with the following criteria: 0.35 mag < g-r < 0.75 mag, −0.1 mag < r-z < 0.8 mag, ellipticity < 0.4, and FWHM < 1.35 arcsec.

In Fig. A.1, we plot the photometric errors for all detected sources in our data, as a function of their magnitude, in the upper panels for each of the g, r, and z bands. In the lower panels, we plot the histogram of sources compatible with GC candidates within three times the effective radius of the main model, as discussed in Section 3.2. Additionally, we indicate the expected position for the peak in magnitude of the GC luminosity function (GCLF) for an object located in the Virgo cluster, and thus

at a distance of 16.5 Mpc (distance modulus of 31.09 mag). We used as our reference the value provided by Rejkuba (2012) in the V band, adapted to the SDSS r band by Román et al. (2019) for a diffuse dwarf of similar morphology and stellar mass to UGC 7346. To obtain the peak values of the GCLF in the g and z bands we used the colours of the main model, as discussed in Section 3.1.

Because the selection of GC candidates was performed using a residual $g + r$ sum image to calculate photometric magnitudes in g, r, and z bands – and additionally for a GC candidate to be selected it requires reliable photometry in all three bands – a strict completeness analysis is very complex. However, the magnitude histograms of the selected GC candidates provide useful information. The vast majority of the GC candidates detected are in the bright half of the GCLF. We also find that the brightest GCs would be found at a distance of about 1 mag from the GCLF peak in the three bands, g, r, and z. This is as expected since, for the stellar mass of UGC 7346, one sigma of the GCLF will be on the order of (or below) 1 mag (Jordán et al. 2007; Villegas et al. 2010). This provides additional evidence that we are indeed detecting GCs in UGC 7346.
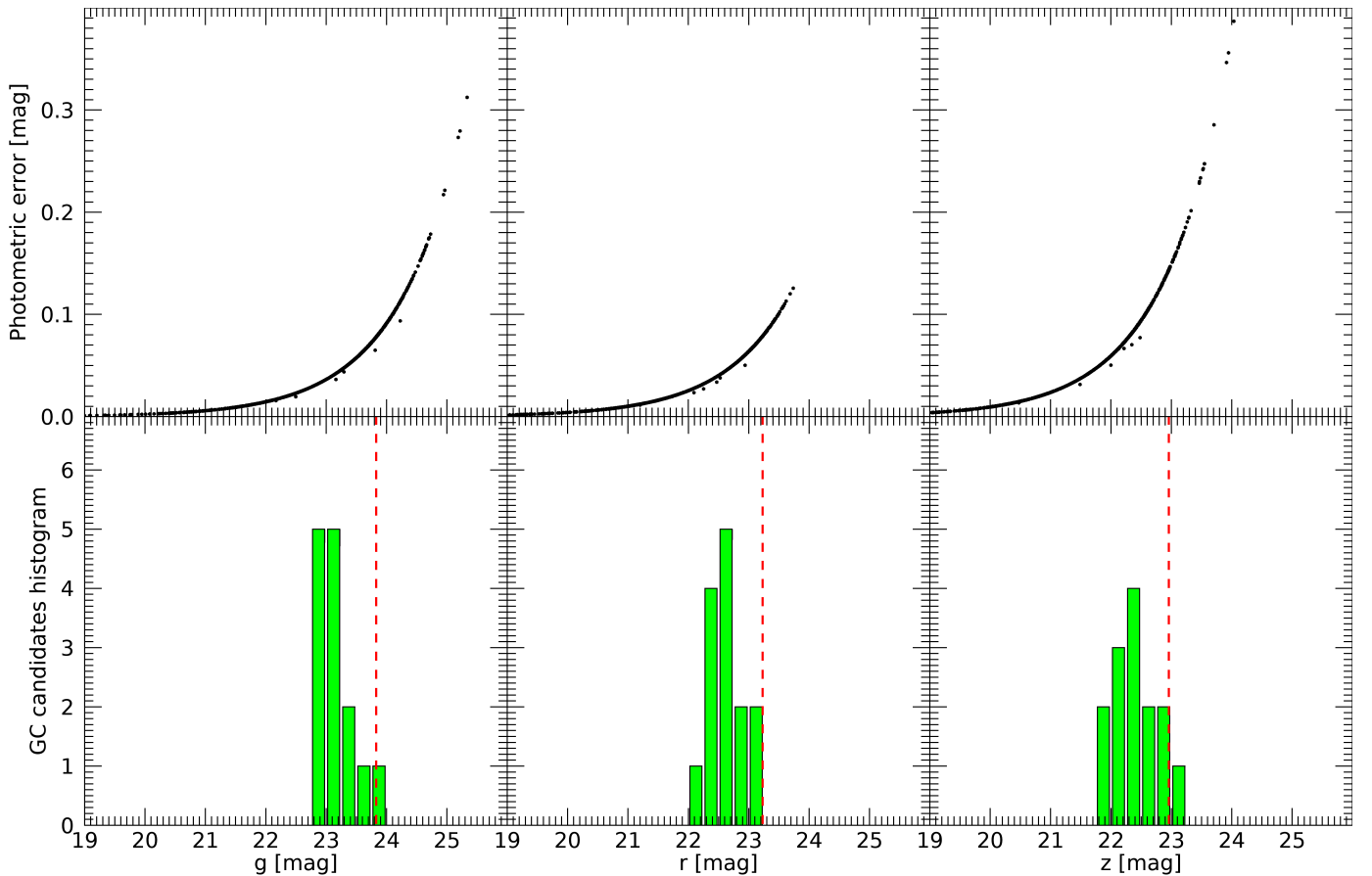

Fig. A.1. Upper panels: Photometric errors in aperture photometry (see text) for sources in the field of UGC 7346 for the g, r and z bands. Lower panels: Magnitude histograms for the GC candidates of UGC 7346. The expected peak of the GCLF is marked by a red dashed line.

Table A.1. Coordinates and photometric magnitudes of the GC candidates in UGC 7346 located within three effective radii.

R.A. (J2000)	Dec. (J2000)	g	r	z
[deg]	[deg]	[mag]	[mag]	[mag]
GCs within 1 effective radius				
184.6764	17.7147	23.71 ± 0.07	23.07 ± 0.07	23.06 ± 0.16
184.6729	17.7150	23.19 ± 0.04	22.57 ± 0.04	22.53 ± 0.10
184.6743	17.7159	23.45 ± 0.06	22.91 ± 0.06	22.89 ± 0.13
184.6743	17.7169	22.76 ± 0.03	22.32 ± 0.03	22.08 ± 0.06
184.6757	17.7199	23.18 ± 0.04	22.67 ± 0.05	22.24 ± 0.07
184.6699	17.7193	22.90 ± 0.03	22.25 ± 0.03	21.86 ± 0.05
184.6735	17.7190	23.24 ± 0.05	22.68 ± 0.05	22.31 ± 0.08
184.6719	17.7208	23.48 ± 0.06	22.81 ± 0.05	22.56 ± 0.10
184.6740	17.7210	22.96 ± 0.03	22.27 ± 0.03	21.80 ± 0.05
GCs within 1 and 3 effective radius				
184.6971	17.7123	22.88 ± 0.03	22.53 ± 0.04	22.36 ± 0.08
184.6667	17.7123	22.87 ± 0.03	22.31 ± 0.03	22.32 ± 0.08
184.6978	17.7190	23.21 ± 0.04	22.54 ± 0.04	22.41 ± 0.09
184.6578	17.7200	23.07 ± 0.04	22.45 ± 0.04	22.19 ± 0.07
184.6849	17.7417	23.83 ± 0.08	23.18 ± 0.07	22.84 ± 0.13